GEOPHYSICS, VOL. 64, NO. 4 (JULY-AUGUST, 1999); P. 1239–1246, 7 FIGS.

Imaging structures below dipping TI media

Robert W. Vestrum*, Don C. Lawton‡, and Ron Schmid*

ABSTRACT

Seismic anisotropy in dipping shales causes imaging and positioning problems for underlying structures. We developed an anisotropic depth-migration approach for *P*-wave seismic data in transversely isotropic (TI) media with a tilted axis of symmetry normal to bedding. We added anisotropic and dip parameters to the depth-imaging velocity model and used prestack depth-migrated image gathers in a diagnostic manner to refine the anisotropic velocity model.

The apparent position of structures below dipping anisotropic overburden changes considerably between isotropic and anisotropic migrations. The ray-tracing algorithm used in a 2-D prestack Kirchhoff depth migration was modified to calculate traveltimes in the presence of TI media with a tilted symmetry axis. The resulting anisotropic depth-migration algorithm was applied to physical-model seismic data and field seismic data from the Canadian Rocky Mountain Thrust and Fold Belt. The anisotropic depth migrations offer significant improvements in positioning and reflector continuity over those obtained using isotropic algorithms.

INTRODUCTION

Dipping anisotropic strata overlying a target of interest can be characterized as a lens for propagating seismic energy. Below this lens, dipping as well as horizontal reflectors at boundaries between isotropic strata will be incorrectly positioned if isotropic models are assumed during data processing—particularly depth migration. Whereas isotropic depth migration corrects imaging problems and positioning errors associated with lateral, but isotropic, velocity heterogeneity, anisotropic depth migration is required to correctly locate images when transversely isotropic (TI) strata with a dipping axis of symmetry are present.

Larner and Cohen (1993) and Alkhalifah and Larner (1994) document migration errors in TI media. Uzcategui (1995) and Alkhalifah (1995) address the problem of depth imaging in the presence of vertical transverse isotropy (VTI). Kitchenside (1992), Ball (1995), and Vestrum and Muenzer (1997) address seismic imaging in the presence of tilted transversely isotropic (TTI) media. Isaac and Lawton (1999) show dramatic positioning errors of horizontal reflectors below TI media with a tilted symmetry axis. In this paper, we illustrate an instance in which anisotropic depth migration is necessary to create an accurate depth image of physical seismic modeling data. We also apply anisotropic depth migration to a seismic data set from the Canadian Rocky Mountain Foothills.

In this approach, we do not attempt to derive physical properties of individual stratigraphic layers; rather, we find anisotropic parameters for large intervals in our velocity model that offer the best seismic depth image. The approach to the TTI problem presented here is based on traditional prestack depth migration analysis. Inspection of prestack image gathers from the resulting anisotropic depth migration directs modification of the anisotropic velocity model. Image-gather analysis for anisotropic depth migration is similar to the analysis used commonly in isotropic depth migration, except that additional anisotropic parameters in the velocity model are estimated.

ANALYTIC BACKGROUND

Clastic sediments, particularly shales, typically exhibit transverse isotropy, where *P*-wave seismic velocity is constant in all directions parallel to bedding and typically slower in all other directions. Dipping anisotropic strata in the overburden cause mispositioning errors on seismic reflectors below (Di Nicola-Carena, 1997; Leslie et al., 1997; Vestrum and Muenzer, 1997).

Thomsen (1986) defines a simple and useful method for parameterizing a TI medium. The weak anisotropy approximation using Thomsen's parameters [equation (1)] gives the phase velocity, v, as a function of phase angle, θ, from the symmetry axis or bedding-plane normal:

Presented at the 67th Annual Meeting, Society of Exploration Geophysicists. Manuscript received by the Editor January 27, 1998; revised manuscript received January 13, 1999.
*Kelman Seismic Processing, 600-540 5th Ave. SW, Calgary, Alberta T2P 0M2, Canada; e-mail: robv@kelman.com; ron@kelman.com.
‡Dept. of Geology and Geophysics, Univ. of Calgary, 2500 University Drive NW, Calgary, Alberta T2N 1N4, Canada; e-mail: donl@geo.ucalgary.ca.

$$v(\theta) = v_0(1 + \delta \sin^2\theta \cos^2\theta + \varepsilon \sin^4\theta), \quad (1)$$

where v_0 is the velocity normal to bedding, δ determines how fast or slow the P-wave velocity propagates at small angles oblique to the symmetry axis, and ε is approximately the fractional difference between the velocities parallel and perpendicular to bedding. While Thomsen's approximation is for weak anisotropy, the parameters v_0, ε, and δ may be used to describe P-wave velocities and other kinematic signatures for TI media with any strength of anisotropy (Tsvankin, 1996).

Figure 1 illustrates a propagating wavefront in a TI medium with a tilted axis of symmetry. The sideslip velocity, $\vec{s}$, is the rate at which energy moves transverse to the wavefront (Dellinger, 1991). Adding the sideslip-velocity and phase-velocity vectors yields the group velocity, $\vec{g}$, or velocity of energy transport (in a lossless medium) away from the source. The equation for the magnitude of $\vec{s}$, which is obtained by differentiating equation (1) with respect to θ, is

$$s \equiv \frac{\partial v}{\partial \theta} = v_0[2\delta(\cos^3\theta \sin\theta - \cos\theta \sin^3\theta) + 4\varepsilon \cos\theta \sin^3\theta]. \quad (2)$$

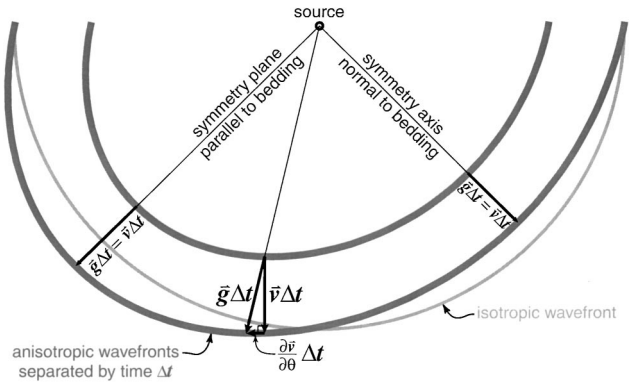

FIG. 1. Wavefronts separated by time Δt. The group velocity $\vec{g}$ is the velocity of energy propagation, and the phase velocity $\vec{v}$ is the velocity normal to the wavefront. The distance between wavefronts normal to the wavefront is $\vec{v}\Delta t$, and the distance between wavefronts in the direction away from the source is $\vec{g}\Delta t$.

This relationship between phase and group velocity is shown in equations (3) and (4). Equation (3) gives the relationship between the magnitudes of the phase and group velocity vectors. Equation (4) gives the relationship between the angles of the two vectors relative to the symmetry axis (i.e., normal to bedding):

$$g = \sqrt{v^2 + \left(\frac{\partial v}{\partial \theta}\right)^2} \quad (3)$$

and

$$\phi = \theta + \arctan\left[\frac{(\partial v/\partial\theta)}{v}\right], \quad (4)$$

where ϕ is the angle between the group-velocity vector and the symmetry axis and θ is the angle between the phase-velocity vector and the symmetry axis.

It is convenient to define sideslip distance, S, as a function of the vertical thickness of the dipping anisotropic strata, T, and the magnitudes of the sideslip velocity, s, and the phase velocity v:

$$S \equiv \frac{s}{v}T. \quad (5)$$

The sideslip distance is the displacement of a reflection point from the common midpoint for a horizontal reflector below a layer of vertical thickness T with a tilted axis of symmetry. It is the lateral mispositioning error shown in Figure 2.

Figure 3 is a plot of S normalized by T as a function of both dip of the anisotropic strata and δ for $\varepsilon = 0.1$ in the zero-offset case. The phase angle for a zero-offset reflection from a horizontal reflector is 0° from vertical; therefore, the phase angle

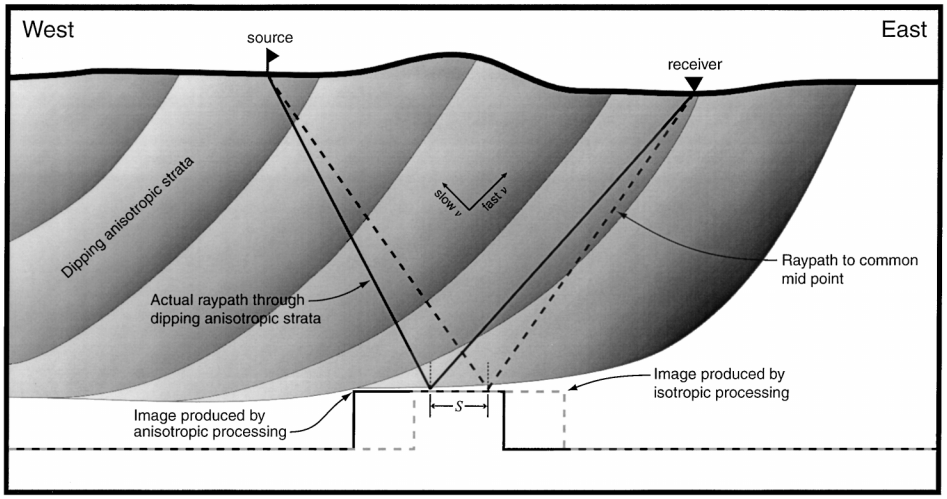

FIG. 2. Cross-section showing lateral movement predicted from isotropic processing of data where transverse isotropy with a tilted axis of symmetry is present. The dashed lines represent the result of isotropic processing. S is the distance between the actual subsurface reflection point and the reflection point when isotropy is assumed.

from the axis of symmetry, θ, is equal to the dip for the zero-offset reflection from a horizontal reflector. From this graph we can see, for example, that for a reflector below 1000 m of anisotropic strata dipping at 45° with $\varepsilon = 0.1$, the zero-offset reflection point will be displaced laterally by about 100 m for any value of δ between 0 and 0.1. Figure 3 also shows that δ has a greater impact than ε on reflection-point displacement for dips less than about 20°.

Figure 2 shows the shift one can expect on a subsurface structure below dipping shales. Because the velocity parallel to the shale bedding is higher than the velocity perpendicular to bedding, rays from the eastern or updip side of the structure will travel in the fast direction and rays from the western or cross-dip side of the structure will travel in the slow direction. The least-time raypath will have a longer travelpath in the faster direction, as shown in this figure and predicted by the anisotropic Snell's law (Byun, 1982). If we process these data with an isotropic assumption, the subsurface structure will image in the updip direction of the anisotropic strata from where it is in the subsurface.

Anisotropic depth migration

The only difference between the isotropic and anisotropic Kirchhoff depth migrations implemented in this study is in the traveltime computations. Both algorithms use a traveltime generator that propagates wavefronts from each shot and receiver location through a gridded velocity model. Wavefronts separated by constant time increments populate the velocity field. A migration traveltime field is then calculated by adding the shot and receiver traveltimes at each point in the model. In the isotropic case, each point along the wavefront curve moves forward in the direction normal to the wavefront for each time step in accordance with the model velocity local to that point. We modified the existing traveltime calculator such that anisotropic group velocities, calculated using equations (3) and (4), are used to propagate the wavefront forward each step. In an anisotropic medium, the point on the wavefront moves forward along the group velocity vector, which is generally oblique to the wavefront normal. Once source and receiver traveltimes are calculated, migration operators for a Kirchhoff depth migration are generated from the traveltimes.

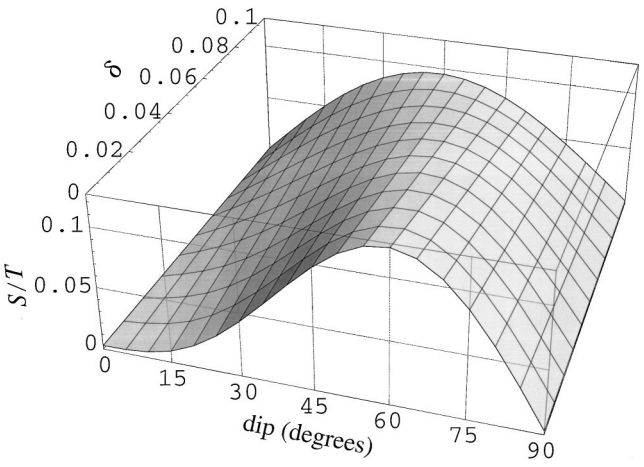

FIG. 3. S/T, the sideslip distance S normalized by vertical thickness of the anisotropic strata T, versus δ and dip of anisotropic strata; $\varepsilon = 0.1$, and the reflector is horizontal. This graph shows the lateral-positioning error we can expect below dipping anisotropic strata. For example, 1 km of shale dipping at 45° will create a lateral-positioning error of approximately 100 m for $\varepsilon = 0.1$ and any value of δ. We can also observe the subtle effect δ has on the lateral-positioning error.

DEPTH IMAGING OF PHYSICAL-MODEL SEISMIC DATA

Seismic data from an anisotropic physical model described by Isaac and Lawton (1999) were used to test the migration. A cross-section of this model is shown in Figure 4a; it consists of a TI overburden layer, 1500 m thick, with the axis of symmetry dipping at 45°. The layer is made of phenolic resin and has parameters $v_0 = 2945$ m/s, $\varepsilon = 0.241$, and $\delta = 0.100$. An isotropic layer of plexiglas containing a fault (Figure 4a) underlies this anisotropic overburden. Isotropic depth migration of the seismic data, shown in Figure 4b, exhibits errors in both depth of horizontal reflectors and position of the fault.

The position error arises because isotropic migration places the reflection point at the midpoint for reflections from horizontal interfaces. The depth error arises because the isotropic imaging velocities (i.e., those velocities which best flatten image gathers) are greater than the vertical velocities in the model. As a result, the reflectors are imaged over 100 m too deep.

The isotropic depth image (Figure 4b) was generated using the optimum imaging velocities, as shown by the flat events in the image gathers displayed on the section. The image gather on the far left shows some residual moveout. The difference in moveout on this gather is likely from the different azimuth distribution on this gather: it is at the downdip end of the line. There are more data migrating into this gather from the fast direction, and the image gather indicates a faster model velocity is required to flatten the gather.

Anisotropic depth migration produced consistently flat prestack image gathers with correct depths, as shown in Figure 4c. In this case, the input to the migration consisted of a grid containing values of v_0, ε, δ, and tilt of the symmetry axis at each node. The grid spacing was 30 m by 50 m in depth. The basement fault is also imaged close to its true position. Although the reflectors have zero dip, the fault (interpreted by the reflection terminations) was moved laterally by 300 m in the anisotropic depth migration (Figure 4c) as compared with the isotropic depth migration (Figure 4b) to be placed in the correct position. Using ε for this material of 0.241, we predicted a sideslip error of 334 m for the zero-offset reflection. There is a difference of 34 m between the lateral-positioning error observed in the multioffset data and the error predicted by calculating the sideslip error for a zero-offset reflection. Some lateral-positioning discrepancies may also be from a misinterpretation of the reflection terminations. There is also a migration artifact on the upper reflection termination that makes it difficult to precisely pick the top edge of the structure.

FIELD DATA EXAMPLE

Anisotropic depth migration was also tested on the Husky/Talisman data set from the southern Alberta Foothills, described by Stork et al. (1995). This line runs over rough topography with dipping reflectors coming to surface (Lines et al., 1996). The upper 2.5 km of section is shale-dominated clastics, and the lower part of the section is mostly carbonates.

Although anisotropic velocities are suspected in the upper clastic section, we are concerned particularly about imaging below the dipping strata. The result of an isotropic depth migration of this section is displayed, in time, in Figure 5.

During isotropic depth-migration velocity analysis, we first observed that the image gathers were flat below flat-lying strata in the overburden but showed significant residual moveout beneath steeply dipping strata. Identical stratigraphic units required a much higher model velocity when these units were dipping steeply. We felt that using velocity gradients such that steeply dipping rocks had a higher model velocity than the same rocks with zero dip was not geologically justified. Figure 6a

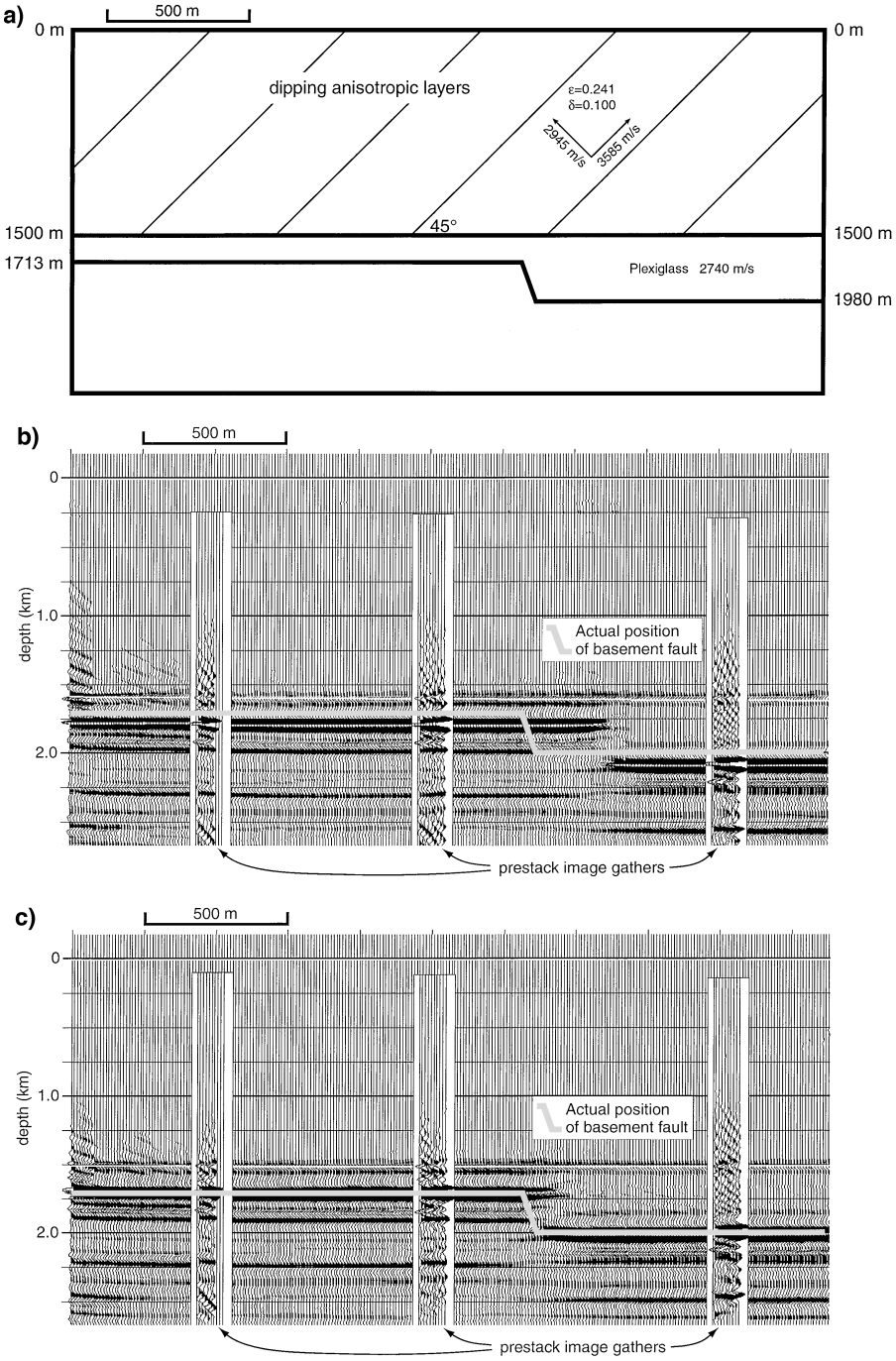

FIG. 4. (a) Anisotropic physical model from the Foothills Research Project. Note the 45° dipping anisotropic overburden above horizontal reflectors. The plexiglas layer is isotropic. (b) This isotropic depth migration yields flat image gathers but incorrect reflector depths and lateral position. (c) The anisotropic image shows flat image gathers with correct depths and improved lateral position.

shows the result of isotropic depth migration of the data set, including image gathers and some selected raypaths of events that contribute to the gathers. The gather on the right of Figure 6a shows residual moveout on the basement reflector. This indicates the dipping zone in the upper part of the section needs a slower velocity to better flatten the gather. The gather in the center, below the steeply dipping shales, shows that the moveout on the basement reflector is significantly overcorrected, indicating the same dipping zone on the model needs a higher velocity to improve the imaging. This conflict in imaging-velocity requirements of the two gathers was reconciled using anisotropic velocities that are laterally consistent, with lower velocities perpendicular to bedding and higher velocities parallel to bedding.

The velocity model was then parameterized for an anisotropic depth migration with the required dip information obtained from the interpretation in Figure 5. Only the shale-dominated clastic layers in the upper part of the section were considered anisotropic in our model. We used parameters determined from refraction-survey measurements on near-vertical shales by Leslie and Lawton (1998) on dipping shales in the Alberta Foothills to help us constrain the anisotropic velocity model. In two separate field locations, δ was found to be near zero for an ε of 0.14 and 0.26. Since δ is small and changes in δ have a subtle influence on s, we parameterized our model with ε. We set δ to be one-quarter of ε and iterated to find the ε that produced the flattest prestack image gathers. If possible, a complete anisotropic velocity model should contain estimates for both δ and ε.

Initial values of anisotropic parameters were $\varepsilon = 0.15$ and $\delta = 0.038$, based on field measurements by Leslie and Lawton (1998) for similar rocks, and the initial v_0 was based on an isotropic depth-migration velocity analysis beneath the horizontal anisotropic layers. After a few revisions to the model, guided by the inspection of image gathers, optimum imaging was achieved for $\varepsilon = 0.10$ and $\delta = 0.025$. Once the image-gather conflict shown in Figure 6a was resolved, we inspected the image gathers again for improvements in flatness of gathers with a change in v_0.

With the anisotropic migration (Figure 6b), imaging was improved below the dipping strata without compromising image quality below horizontal strata. The laterally varying dip was advantageous in refining the anisotropic model parameters. When confronted with residual moveout on an image gather, we had difficulty deciding whether to change v_0 or ε and δ to flatten the gather. By assuming that the properties of the strata do not change with dip, however, only a limited range in v_0, ε, and δ could result in a good image below both flat-lying and steeply dipping strata. Although the solution is not unique, the resulting image is better than that obtained from isotropic migration.

A comparison between the final anisotropic depth migration and the final isotropic depth migration is shown in Figure 7. Differences observed between the sections are attributed only to differences between the isotropic and anisotropic migrations.

The highlighted rectangles on both sections in Figure 7 show some of the key improvements of anisotropic depth migration when compared to isotropic depth migration. Boxes A and A′ show differences beneath the dipping strata; there is a lateral movement and improvement in reflector continuity below the fault contact in the upper left corner of A′ compared with that of A. The reflector that spans the bottom of A′ also shows improved continuity. The anticline interpreted in box B (Figure 7a) is not present in B′ (Figure 7b). The anticline in B is considered to be a false depth structure caused by a significant change in near-surface dips. Basement reflector continuity is also improved after anisotropic depth migration, as evident by comparing boxes C and C′.

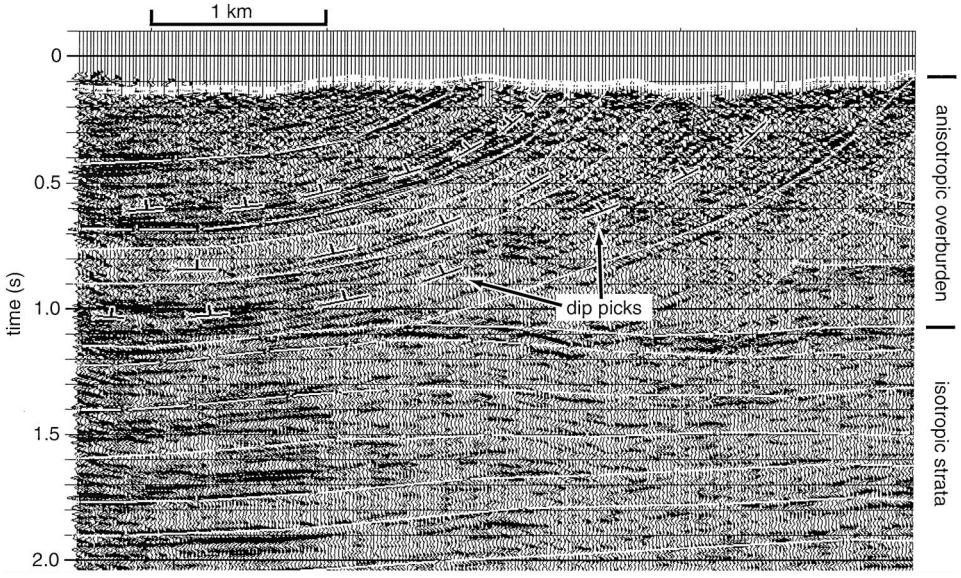

FIG. 5. Interpreting dip from the seismic section. The white lines on the section are velocity-model zone boundaries. The dip is allowed to vary laterally within a zone, as shown here. The upper section contains the shale-dominated clastic sequence; the lower section contains carbonates, assumed to be isotropic in our velocity model.

Thus, the depth-migrated sections in Figure 7 show a significant improvement in image quality when seismic anisotropy is taken into account, and demonstrate the need for anisotropic depth migration in areas of complex geological structure.

CONCLUSIONS

We draw the following conclusions from this study:

1) an isotropic assumption causes mispositioning of imaged structures below dipping anisotropic strata because sideslip is ignored;
2) we carried out anisotropic traveltime calculations to account for sideslip in anisotropic depth migration;
3) for anisotropic strata dipping at angles near 45°, ε has a greater influence on sideslip than does δ;
4) tests using the anisotropic migration on physical-model seismic data resulted in flat image gathers and more accurate target depths and positions than did isotropic migration; and
5) application of the anisotropic depth migration to field data using focusing criteria to interpret the anisotropic model produced a depth image with image quality superior to that of the isotropic migration.

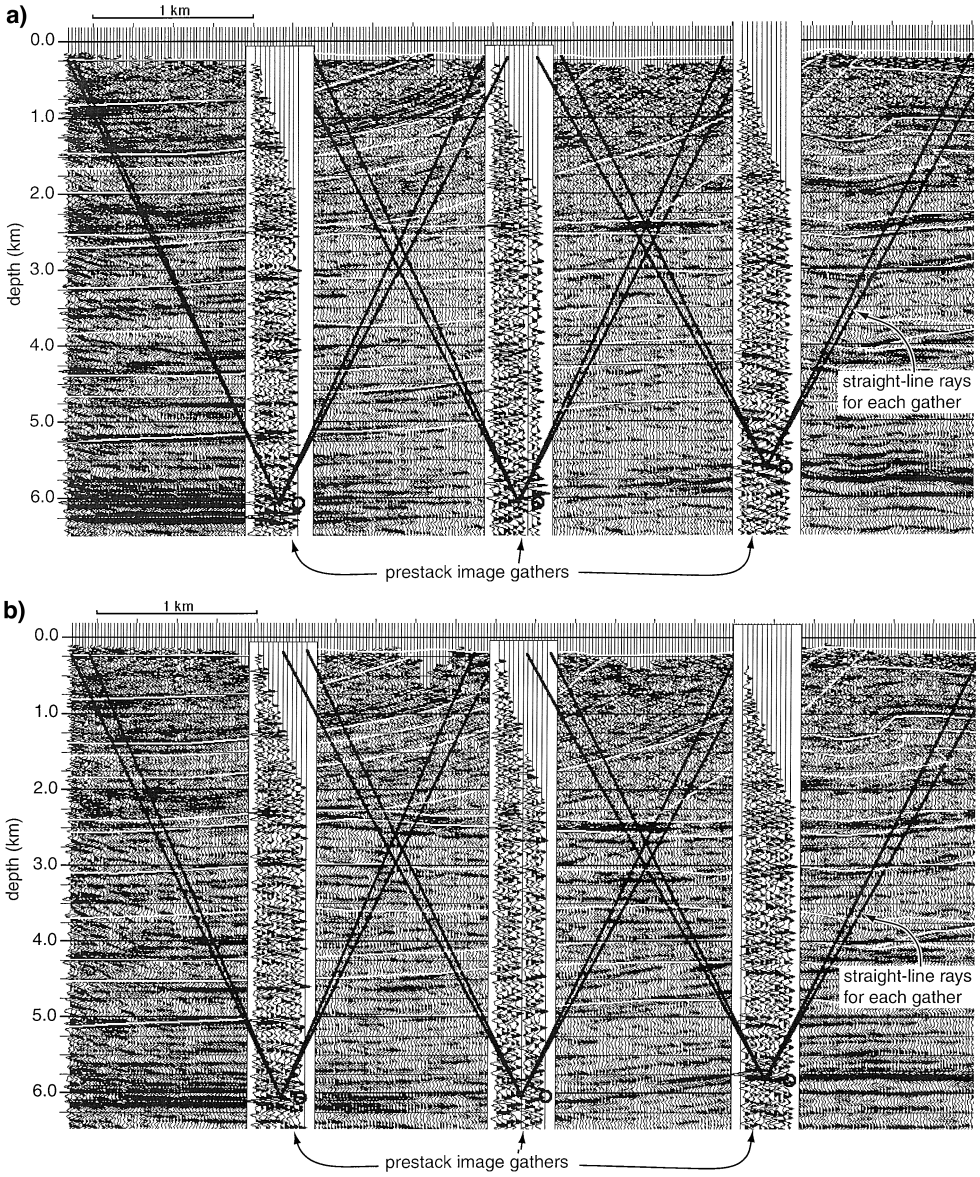

FIG. 6. (a) Image-gather displays for the isotropic model. The gather in the center is overcorrected; therefore, a faster model velocity is needed to flatten it. The gather on the right is undercorrected and needs a slower velocity. The black lines represent a straight-line approximation of ray tracing to the basement reflector at 3 km. Note that both the center gather and the right gather contain seismic energy that traveled through the same clastic layers between the two gathers and above 2.4 km depth. The gather on the right contains energy that traveled normal to bedding—the slow-velocity direction. The gather in the center contains energy that traveled parallel to bedding—the fast-velocity direction. (b) Image-gather displays for the anisotropic velocity model. Model parameters $\varepsilon = 0.1$ and $\delta = 0.025$ are used for the clastic layers in the upper 2.5 km of the section. The gather in the center has improved relative to the same gather in (a), and the reflector on the stack at 3 km shows improved continuity. The gather on the right is flat—again, an improvement over the same gather in (a).

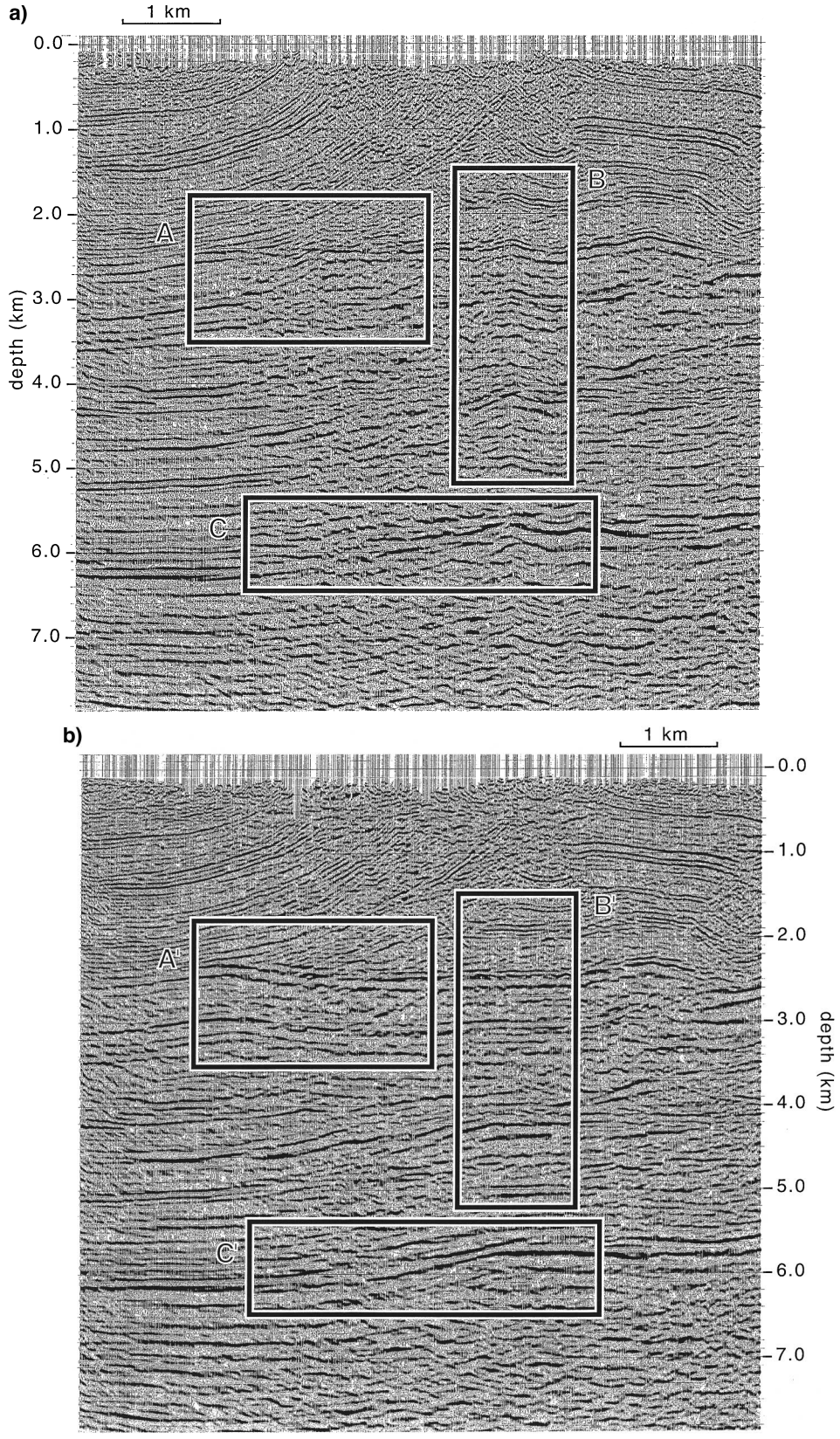

FIG. 7. (a) Final depth-migrated image using the isotropic model. Note the lack of continuity in boxes A and C and the structures on several reflectors in B for comparison with the boxes in (b), the final depth-migrated image using the anisotropic model with $\varepsilon = 0.1$ and $\delta = 0.025$. The boxes highlight some of the more significant improvements over the standard depth migration in (a). Note the improvement in continuity of reflectors in A′ and C′ over that for A and C, and that the imaged structures in B are flattened in B′.

ACKNOWLEDGMENTS

The authors thank the sponsors of the Foothills Research Project and the Natural Science and Engineering Research Council for their financial support of this research and Kelman Seismic Processing for data processing services. We also thank Ken Larner, Ilya Tsvankin, and an anonymous reviewer for their constructive reviews of this paper.

REFERENCES

Alkhalifah, T., 1995, Gaussian beam depth migration for anisotropic media: Geophysics, **60**, 1474–1484.

Alkhalifah, T., and Larner, K., 1994, Migration error in transversely isotropic media: Geophysics, **59**,1405–1418.

Ball, G., 1995, Estimation of anisotropy and anisotropic 3-D prestack depth migration, offshore Zaire: Geophysics, **60**, 1495–1513.

Byun, B. S., 1982, Seismic parameters for media with elliptical velocity dependencies: Geophysics, **47**, 1621–1626.

Dellinger, J., 1991, Anisotropic seismic wave propagation: Ph.D. thesis, Stanford Univ.

Di Nicola-Carena, E., 1997, Solving lateral shift due to anisotropy: 67th Ann. Internat. Mtg., Soc. Expl. Geophys., Expanded Abstracts, 1525–1528.

Isaac, J. H., and Lawton, D. C., 1999, Image mispositioning due to dipping TI media: A physical seismic modeling study: Geophysics, **64**, 1230–1238, this issue.

Kitchenside, P. W., 1992, An implementation of anisotropic migration: Some issues and examples: 54th Mtg., Eur. Assoc. Expl. Geophys., Abstracts, **92**, 234–235.

Larner, K., and Cohen, J. K., 1993, Migration error in transversely isotropic media with linear velocity variation in depth: Geophysics, **58**, 1454–1467.

Leslie, J., and Lawton, D. C., 1998, A refraction seismic field study to determine the anisotropic parameters of shales: The Leading Edge, **17**, 1127–1129.

Leslie, J., Lawton, D. C., and Cunningham, J. D., 1997, A refraction seismic field method to determine the anisotropic parameters of Wapiabi shales: Proc. 1997 National Meeting, Can. Soc. Expl. Geophys., 61–63.

Lines, L., Wu, W., Lu, H., Burton, A., and Zhu, J., 1996, Migration from topography: Experience with an Alberta Foothills data set: Can. J. Expl. Geophys., **32**, 24–30.

Stork, C., Welsh, C., and Skuce, A., 1995, Demonstration of processing and model building methods on a real complex structure data set: Ann. Conv., Workshop 6, Soc. Expl. Geophys., Proceedings.

Thomsen, L., 1986, Weak elastic anisotropy: Geophysics **51**, 1954–1966.

Tsvankin, I., 1996, *P*-wave signatures and notation for transversely isotropic media: An overview: Geophysics, **61**, 467–483.

Uzcategui, Omar, 1995, 2-D depth migration in transversely isotropic media using explicit operators: Geophysics, **60**, 1819–1829.

Vestrum, R. W., and Muenzer, K., 1997, Imaging below dipping anisotropic shales: Proc. 1997 National Meeting, Can. Soc. Expl. Geophys., 64–65.